# Electronic properties of polyethylene naphthalate as derived from photo-stimulated discharge, luminescence experiments and quantum chemical calculation

Duvan Mendoza Lopez, Gilbert Teyssedre, Laurent Boudou, Laurent Berquez, Christian Laurent, Shinya Iwata, Tatsuo Takada

# Electronic properties of polyethylene naphthalate as derived from photo-stimulated discharge, luminescence experiments and quantum chemical calculation

Duvan Mendoza Lopez[1], Gilbert Teyssedre[1*], Laurent Boudou[1], Laurent Berquez[1], Christian Laurent[1], Shinya Iwata[2], Tatsuo Takada[3]

[1]LAPLACE, University of Toulouse, UPS and CNRS, Toulouse, France.
[2]Osaka Research Institute of Industrial Science and Technology, 594-1157, Osaka, Japan
[3]Tokyo City University, Tamazutsumi, Setagaya, 158-8557, Tokyo, Japan

*Corresponding author: gilbert.teyssedre@laplace.univ-tlse.fr

***Cite as:*** D. Mendoza Lopez, G. Teyssedre, L. Boudou, L. Berquez, C. Laurent, S. Iwata, T. Takada, "Electronic properties of polyethylene naphthalate as derived from photo-stimulated discharge, luminescence experiments and quantum chemical calculation", J. Phys. D: Appl. Phys. 57, 315502-1/14, 2024. DOI: 10.1088/1361-6463/ad415b

***Abstract-*** The electronic properties of thin films of Poly(ethylene 2,6-naphthalate) –PEN, are investigated based on their photo-physical (optical absorption, photoluminescence) and electrical (space charge distribution, photo-stimulated discharge) behavior. Photo-stimulated currents are associated with optical absorption of the material leading to space charge dissipation as demonstrated by space charge distribution measurement. Based on this set of experimental results and quantum chemical calculation performed on PEN macromolecular system, we propose a new scheme for the electronic levels of PEN. This scheme allows understanding the mechanisms at play in photo-stimulated discharge. One of the main conclusions of our work is that photo-stimulated current measurements do not probe the energy level of traps. Detrapping of charges results from a two-step process where the photon energy is absorbed by chromophores that restitute a part of this energy to trapped charges through various mechanisms. Moreover, the new scheme allows discussing the components of the luminescence excited under different stresses, being electric field, electronic and UV irradiation, charge recombination and thermal activation.

## I INTRODUCTION

Poly(ethylene 2,6-naphthalate) -PEN is an unsaturated polyester widely used in electrical and electronics industry. PEN films are used in applications such as insulation tapes, capacitors, photovoltaic panels, and flexible printed circuits for example. Its relative strong luminescence properties are used for application as scintillator [1]. Thin film PEN capacitors offer the advantage over many other polymers of high temperature stability [2]. Capacitor applications are certainly those requiring the greatest breakdown field for insulating polymers application and understanding the limits of materials require a good knowledge of the electronic properties. Indeed, trapping and detrapping of electronic charges as well as their recombination are controlling high-field properties of dielectrics. Investigation of the electronic energy levels is therefore of prime importance to understand its electrical properties. Space charge and current measurements were reported together with electroluminescence in PEN [3, 4]. Three different conduction regimes were unraveled. A low field, ohmic regime (< 80 kV/mm) with no detectable space charge, an intermediate regime (80 kV/mm < E < 150 kV/mm) with space charge in the electrode vicinity of anode and cathode, and a third regime (E > 150 kV/mm) with onset of electroluminescence being proportional to the strongly non-linear conduction current. An important scientific question is the significance of EL onset and of the non-linear conduction regime. If this threshold represents a degradation threshold, it would then correspond to an upper design field in capacitor application. For these reasons, the photo-physical properties of PEN need specific attention as it may inform on processes at play under high field.

The optical absorption spectrum was reported for PEN molecules in solvent [5] and for thin films [6], and assigned to electronic transitions of the PEN molecules which are a property of delocalized π orbitals of the double phenyl ring and ketone. Photoluminescence was thoroughly investigated [7, 8] and both fluorescence and phosphorescence were reported and related to the unsaturation of the molecule. Photo-stimulated discharge (PSD) is a technique by which a material charged under an electric field is subsequently irradiated by photons of different wavelengths and the external current measured [9, 10]. The processes involved in PSD encompass de-trapping of injected space charges, photoemission from electrodes and polymers, i.e. all the processes involved in photo-conduction experiments [3], the main difference between the two kinds of experiments being the electric field generated either through the applied voltage or through space charge effects. It was proposed that the presence of peaks in the external current when changing the irradiation energy gives an access to the depth of traps. The method was recently discussed in a review paper [11] and one of the open questions concerns the trap depths of several eV that are derived, far above those obtained from other methods like thermo-stimulated currents, surface potential decay, or thermo-luminescence. Indirect effects of optical excitation may be at play, and the direct correlation between excitation wavelength and trap energy may be misleading. Indeed, the coupling between exciton formation, quenching, and generation of charge carriers in organic materials is extremely complex with many potential routes [12, 13].

In this paper, we confirm that irradiating PEN films previously charged under a DC field with photons of different wavelengths result in sample discharging. This is evidenced by simultaneous measurements of space charge distribution by the Laser Induced Modulation Method (LIMM), sample irradiation and external current measurement. The set-up and the experimental measurement protocol constitute a unique system for investigating the relationship between photon irradiation and sample discharge. PSD spectra are subsequently analyzed based on the PEN optical absorption spectrum demonstrating that each PSD peak is associated with a given absorption band. This impacts directly the interpretation usually given for the PSD peaks where trapped charges are released upon irradiation giving a direct access to trap depths. Conversely, photon irradiation generates excited states of the π orbitals through optical absorption. This finding opens a new route for interpreting PSD experiments. Furthermore, we perform quantum chemical calculation [14, 15] on PEN macromolecular system and cross correlate the data with photoluminescence experiments allowing proposing a new scheme for the electronic levels of PEN. On this basis, we are able to revisit the mechanisms at play in PEN luminescence excited by different sources, either non-degradative (charge recombination, mild UV irradiation, thermal activation) or degradative (high field application, electronic irradiation and UV irradiation). The new scheme gives a unique picture of the luminescence of PEN excited in different conditions.

## II METHODS

### Samples

PEN films used for all the experiments were provided by Teijin company under reference Teonex-Q51. Samples are biaxially oriented semicrystalline films, with a crystallinity degree of about 40% [16]. The reported glass transition temperature is of 122°C and the melting point 269°C. The thickness was chosen as to adapt to the method; the size of samples was typically 8 cm in diameter. For space charge and PSD measurements the films were 12 µm in thickness. UV-vis transmission measurements were realized on thinner films (6 µm). Finally, all luminescence experiments were achieved on 25 µm thick films.

### Space charge and PSD measurements

A set up for simultaneous space charge density profiles and photo-stimulated current measurements was implemented in a unique system combining the Laser Induced Modulation Method (LIMM) for space charge measurement and the PSD technique for trap spectroscopy. An innovation of the test bench is the switch from one measurement to the other without moving the sample and the connections. Complete galvanic isolation is achieved by a controlled magnetic switch that allows the selection of one of the techniques depending on a predefined measurement program. Details of the combined test bench are given in [17].

A 50 nm thick, finger shaped gold electrode was sputtered on the surface (front electrode) that receives the thermal (space charge by LIMM) and optical disturbances (PSD measurements). The back electrode is a sputtered film of gold. Front and back electrodes are connected to the HVDC source and the ammeter respectively. A 100

mW 660 nm modulated laser diode is used in the frequency range from 10 Hz to 10 kHz for space charge measurement using Laser Induced Modulation Method [18]. Note that LIMM is sensitive near the irradiated electrode (some µm) with a micrometer resolution. It hardly gives access to space charge density in the depth.

PSD measurements use a monochromatic light produced by a 150 W xenon arc lamp associated with a 1200 gr/mm monochromator with entrance and exit slits of 2 mm producing a spectral bandwidth of 7 nm. Charge accumulation and de-trapping phenomena are recorded following a protocol where a field of 40 kV/mm (positive poling of the irradiated electrode) is first applied for 60 min. The sample is subsequently depolarized for 120 min. Irradiation is effective after 60 min in depolarization, for a duration of 60 min (PSD scan between 600 to 190 nm for 30 min followed by a constant irradiation at 210 nm for 30 min). The field is further increased by step of 40 kV/mm up to 200 kV/mm following the same measurement protocol. The polarity of the voltage applied to the irradiated electrode is subsequently reversed (negative poling) starting at -40 kV/mm, up to -200 kV/mm. Further experimental details are given in [10].

**UV-vis transmission and luminescence experiments**

Optical absorption measurements were achieved in transmission mode on solid films using a HP 8452A apparatus equipped with a Deuterium lamp allowing transmission measurements from 190 to 800 nm.

All the luminescence experiments were realized with a home-made set-up build around a cooled photomultiplier (Hamamatsu R943-02) working in photon counting mode and a cooled CCD camera associated with a grating monochromator for spectra acquisition. An updated description of the set-up is described in [19]. The chamber is designed such as high voltage can be applied, it can sustain secondary vacuum and the sample can be cooled down using liquid nitrogen circulation. Different excitation means of luminescence are exploited, being UV-photons for photoluminescence, electron beam for cathodoluminescence, plasma interaction with the sample surface for charge recombination induced luminescence, etc. Results presented here were already reported for most of them, and reference to initial works is achieved in the following. Samples used are 25 µm thick PEN films.

**Molecular dynamic simulation**

Molecular dynamics (MD) simulations were achieved in order to reproduce the chain configuration of amorphous PEN. This was achieved by condensing 35 monomer units into a pseudo polymer with a density of 1.26 g/cm³, close to that of PEN [15]. The Gromacs 5.0 [20, 21] was used as calculation software for molecular dynamics. MD calculations were achieved in 2 steps consisting in energy minimization followed by force field calculation. Once the structure has been stabilized using these methods, three adjacent molecules were selected and Quantum Chemical Calculation by DFT was performed using Gaussian 09 software. Molecular orbitals of the electron energy levels were derived.

## III RESULTS

**UV-vis spectroscopy**

PEN is a strongly absorbing material in the UV-region. Hence, recording absorption spectra requires working on thin films. Figure 1 shows the absorption spectrum obtained on a 6 µm thick PEN film.

The absorption length $\lambda_e$ was determined using the following relation:

$$A = -log_{10}\left(\frac{I_t}{I_i}\right) \text{ with } \frac{I_t}{I_i} = \exp(-\frac{d}{\lambda_e}) \quad (1)$$

where $I_i$ and $I_t$ are the incident and transmitted light, $A$ is the absorbance and $d$ is the sample thickness. For the derivation of $\lambda_e$, a reflection coefficient of 6% has been taken into account, based on the value of the optical index of 1.65 for PEN [22].

At least four broad absorption peaks are evidenced in the absorption spectrum at about 215/220 nm (5.7/5.6 eV), 240/250 nm (5.1/4.9 eV), 280/300 nm (4.4/4.1 eV), and 340/350 nm (3.6/3.5 eV). Note that similar spectrum was reported for PEN in solution [5]. Moreover, A. Laskarakis et al. computed the absorption spectrum of PEN

using spectroscopic ellipsometry and assigned each absorption to specific electronic transitions in the PEN molecule [6]. The computed values are compared with our own measurements in Table I. They are in reasonable agreement.

The lowest energy peaks (3.5; 3.7; 3.8 eV) are attributed to the electronic transition of the non-bonded electron of the carbonyl O atom from the n state to the π* unoccupied valence state orbital (n→π* transition). The other peaks are split in three components each and correspond to the electronic transition due to the π → π* excitation of the π-electron structures. Because of these features, the PEN films are strongly absorbing and the light penetration depth in the UV region is less than 1 µm.

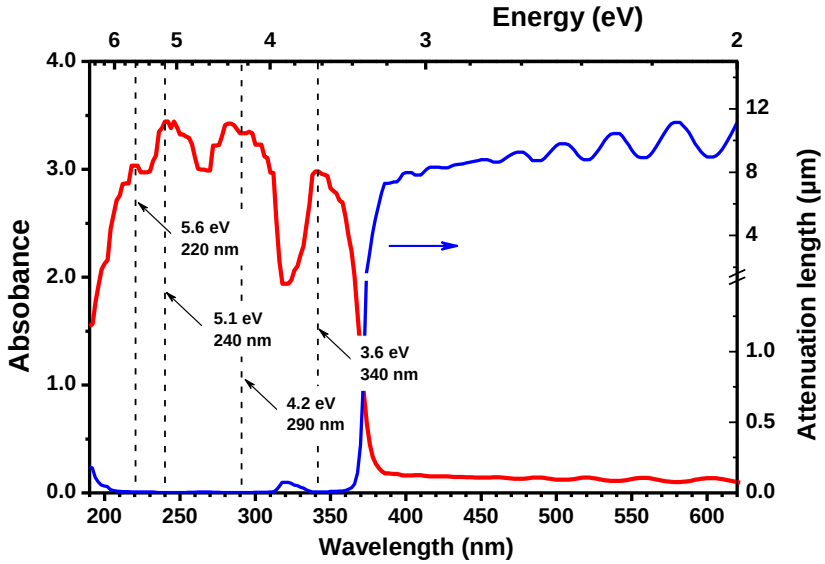


**Fig. 1.** Absorbance and attenuation length spectra obtained for a 6 µm thick PEN film by UV-vis spectroscopy.

### Space charge cartography

A specific protocol, indicated in the top of Fig. 2 was implemented to realize space charge measurements combined with PSD experiments. The indicated field values is applied for 1 h and a volt-off period of 3 h is spent before the next voltage step is applied. During this time, a first series of 6 LIMM experiments are achieved, then the PSD experiment is realized consisting in scanning the irradiation wavelength between 600 to 190 nm for 30 min followed by a constant irradiation at 210 nm for 30 min. Finally, a second series of LIMM measurements are recorded in order to evaluate the impact of the irradiation on the charge distribution. The electric stress was increased from 40 to 200 kV/mm in steps of 40 kV/mm with the positive voltage set to the front electrode, then the complete cycle was repeated for a negative polarity.

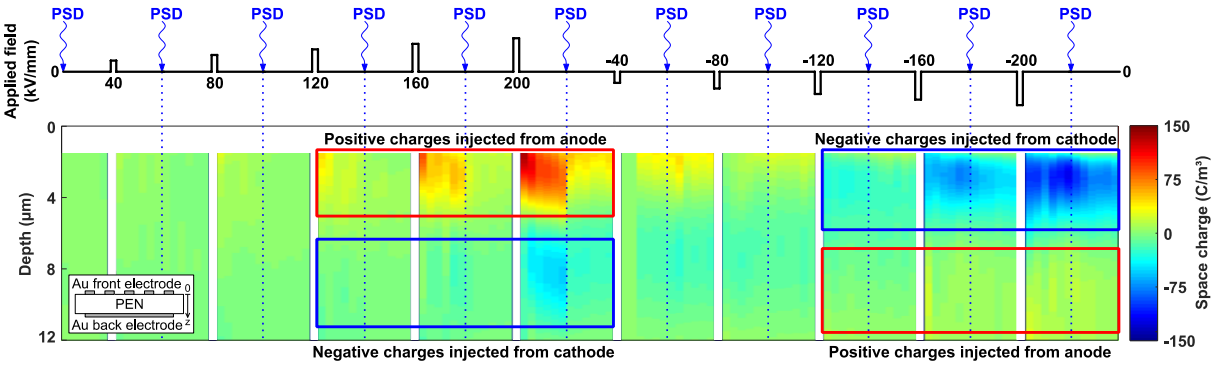


**Fig. 2.** Volt-off LIMM net space charge cartography of a 12 µm-thick PEN sample polarized at different fields (white lines as 1-hour volt-on steps) following the experimental protocol. Irradiation for PSD starts at time indicated by arrows. The space charge cartography is shown from 1.5 µm depth, which is the closest distance from the front electrode that can be accurately represented after signal deconvolution.

The LIMM cartography shown in Fig. 2 reveals the formation of stable positive homocharges when a stress of 80 kV/mm and on is applied. The positive charge stays near the top electrode, even when the polarity is reversed and clear negative charge is set once the field reaches -120 kV/mm. The formation of bipolar domains when the electric field reaches the EL onset (150 kV/mm) is also apparent. This is consistent with the EL excitation mechanism that points towards charge recombination as a major contribution. Note that delayed EL is also operating during relaxation [23] demonstrating the bipolar nature of the space charge and therefore the limitation in accessing the real density of charges. An important feature revealed in Fig. 2 is the space charge relaxation upon irradiation for PSD measurement purpose, with a clear decreasing density of the net charge after irradiation. As expected, the PSD is intrusive vis the charge configuration.

**PSD spectra**

Fig. 3 shows all the PSD spectra obtaining during the full protocol of Fig. 2. The sign of the current is from the lower electrode to the ground (the charging current is positive for a positive voltage applied on the front electrode). As shown in Fig. 3, PSD spectral components are observed at 400 nm (3.1 eV), 360 nm (3.4 eV), 299 nm (4.1 eV), 261 nm (4.7 eV), and 207 nm (6 eV). The appearance and evolution of each peak depends on the applied electric field and its polarity, all being more visible under positive voltage. It is worth pointing out the negative current peaks that persist under polarity reversal when irradiating with 210 nm light for applied fields up to -80 kV/mm. It means that the charge stored under positive voltage has not been released or compensated up to that point.

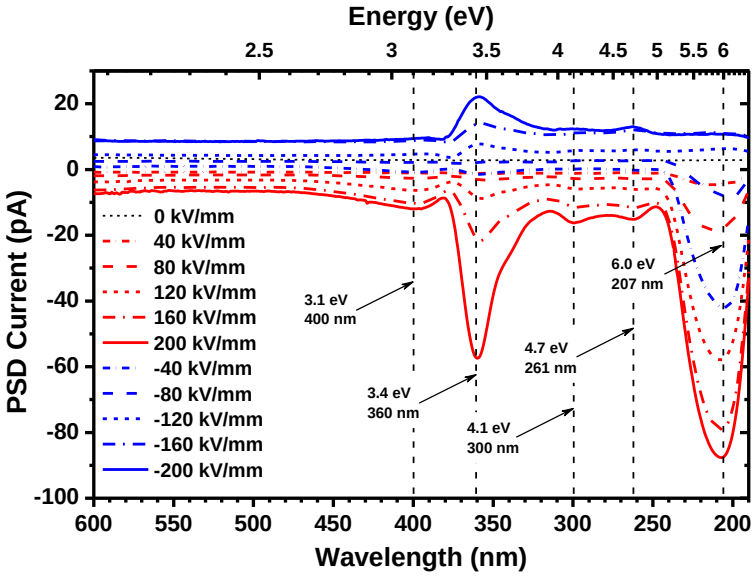


**Fig. 3.** PSD spectra of a 12 µm-thick PEN sample for each volt-off step.

Except for the PSD band at 400 nm, all other features are within a wavelength range where the absorption length does not exceed 1 µm according to UV-vis spectroscopy (Fig. 1). Hence, the discharge in PSD analysis is due to processes occurring in the immediate vicinity of the irradiated electrode.

**Table I.** PSD spectrum, optical absorption and molecular dynamics results.

| PSD peaks (eV) This work | Optical absorption (eV) This work | Optical absorption (eV) From ref. [6] | 3 M -Molecular dynamics. Absorption edges (eV) From ref. [15] | Photoluminescence Emission bands (eV) This work |
|---|---|---|---|---|
| 3.1 (weak) | edge | 3.5; 3.6; 3.8 | 3.0 (level S1) | 3.2; 3.0; 2.9 |
| 3.4 (strong) | 3.4 – 3.6 | | | |
| 3.6 (shoulder) | | | | |
| 4.1 (weak) | 4.0 – 4.4 | 4.1; 4.3; 4.5 | 4.4 (level S2) | |
| 4.7 (weak) | 4.9 – 5.1 | 5.0; 5.1; 5.6 | 6.0 (level S3) | |
| 6.0 (very strong) | 5.6 – 5.7 | | | |

The PSD peak energies are given in Table I. They match with the optical absorption bands of PEN which gives a basis for interpreting the first stage in the process in PSD: the irradiation energy is first used to excite PEN chromophores i.e. electronic excited states are promoted within the band gap. Simulations were carried out to identify the energetics of PEN and the results are presented below.

**MD and DFT calculations for the electronic levels of PEN**

When the MD calculation is performed, the molecule changes shape to an energetically stable configuration due to the temperature and pressure of the system. The calculations are performed at 300 K up to the time the desired density is reached. This step defines a chain configuration. In order to provide a representation of the system as close as possible to the real one and to compute the energy distribution, a configuration with 2 (2M) or 3 (3M) adjacent molecules is considered. The energy levels thus obtained are different from those in an isolated linear PEN chain. Fig. 4-a shows the obtained configuration of 3 adjacent molecules. The shapes of the extracted molecules are randomly arranged. The molecules do not form an ordered cluster, but are arranged in an amorphous form, with variable space between them and with bent parts. The electrostatic forces of the electric dipole created by naphthalene and the carbonyl groups become attractive and repulsive and they are entwined with each other. From there, a charge distribution within the molecule is obtained.

The three-dimensional electrostatic potential distribution of the molecules obtained from the Mulliken charges from which the DFT calculation results is represented in Fig. 4-b. The regions for positive and negative potentials spread and the potential overlaps within the molecules and between the adjacent molecules. It can therefore be inferred that the interaction between the PEN molecules is strong, which can explain the high glass transition temperature (Tg) of the material (based on MD simulations, the calculated Tg is 103 °C; the measured one is around 120 °C).

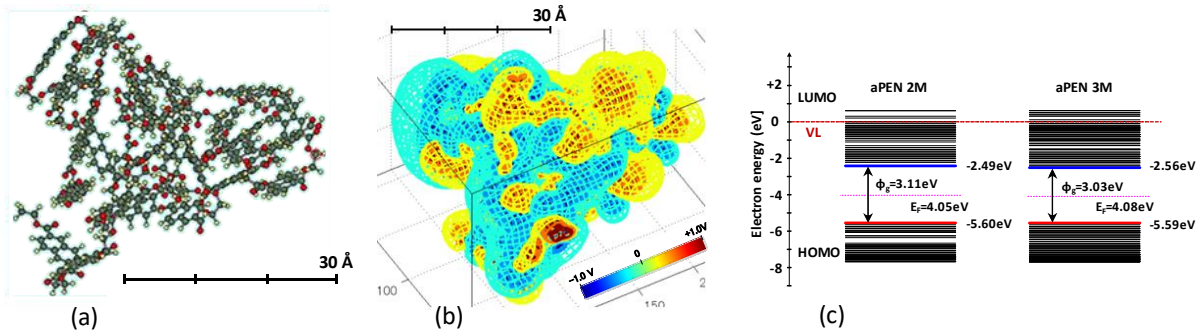


**Fig. 4**. Molecular dynamics and DFT calculation results for PEN: (a) Adjacent molecules configuration; (b) 3D electrostatic potential distribution; (c) Energy levels distribution for '2M' and '3M' molecules

The energy levels obtained for an isolated 5-monomers PEN chain are shown in Fig. 5. Though it is not as representative of a dense material, the energy distribution and electronic transport mechanisms operating within the chain can be discussed. PEN belongs to that group of polymers with the LUMO levels 3 eV below the vacuum level. This is due to the fact that the molecule has a double benzene ring and a ketone in the main chain. The π -electron wave of the conjugated double bonds forms a molecular orbital across the double benzene ring and the ketone on which reside the LUMO and HOMO levels. From the relationship between each energy level and molecular orbital, the energy level of each bonded group is shown in Fig. 5. As molecular orbitals form some sort of localization on conjugated groups, there is no conjugation path along the main chain and LUMO and HOMO levels appear as localized states [24].

Transport along a main chain may occur then by hoping through these localized states. As can be seen in Fig. 5, there are multiple localized levels between the LUMO level and the electronic conduction levels (at approximately 1 eV above the LUMO level). Therefore, the trapped electrons may reach either of these electronic conduction levels while being excited from the localized level. If the excitation probability to level i over an energy difference $\varphi_i$ is:

$$\theta_i = \exp(^{-\varphi_i}/_{kT}) \tag{2}$$

then the effective hopping probability is $\theta_{hop}$ from where an effective electron trapped hole $\varphi_{hop}$ can be deduced from:

$$\theta_{hop} = \sum_i \theta_i = \exp(^{-\varphi_{hop}}/_{kT}) \tag{3}$$

The same reasoning holds for holes hoping from the HOMO level. The hopping barriers so determined appear in Fig. 5c. The effective electron trap depth is 1.26 eV and the potential well seen by holes is 0.72 eV. This particular energy configuration is possibly at the origin of the steep non-linear behavior of the current observed for PEN beyond a threshold field [3, 4]. The lower potential well for holes may imply that the transport current should be dominated by hole transport, at least for what concerns intrachain transport. Space charge measurements realized under fast varying voltage revealed mainly negative charges occupying nearly all the insulation volume [25]. The two features are not necessarily in contradiction since a higher potential well would mean that electrons stay longer in wells, their average velocity would be lower than that of holes, therefore leading to a net negative charge.

For a 5 monomeric units-long PEN molecule, the band gap is 3.61 eV. The energetic levels computed for a group of two or three adjacent molecules, which is a far more realistic situation of the molecules packing in PEN, give band gaps of 3.11 eV and 3.03 eV, respectively, see Fig. 4-c. The substantial reduction in the band gap is due to both to the randomness of chain configuration and chain-chain interactions.

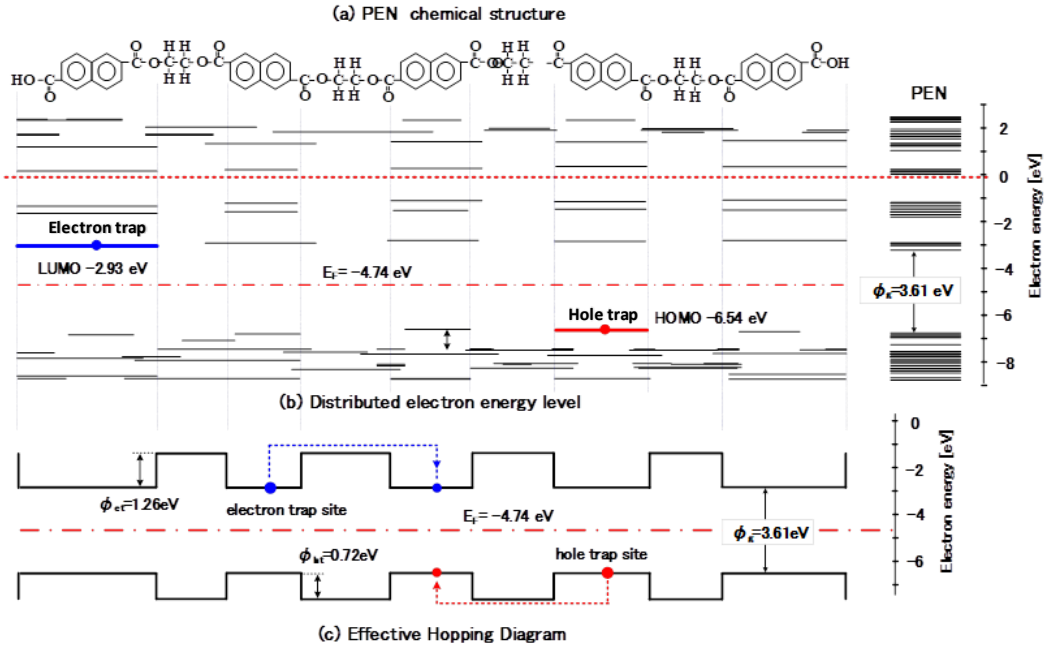


**Fig. 5**. The energy levels of a 5 monomers-long PEN chain obtained by DFT calculation.

## IV DISCUSSION

### Luminescence absorption, emission, and electronic levels of PEN

Optical absorption, emission and band gap are not strictly related as vibronic levels contribute to the distortion of the spectra, with larger main apparent absorption energy and lower emission energy than the band gap. Fig. 6 gives the photoluminescence spectrum of a PEN film and the assignment of the peaks. Measurements were achieved at low temperature (≈-160°C) to reveal the phosphorescence as well as the structure in the fluorescence peak. The main emission peaks at 412 nm (3.01 eV), with shoulders at 390 nm (3.18 eV) and 430 nm (2.88 eV). It is due to $^{1}(\pi, \pi^*)$ fluorescence transition of an excimer state formed between two adjacent naphthalene-dicarboxylate units [26]. The structured nature of the spectra in aromatic carbonyl compounds is related mainly to the vibronic states of the carbonyl groups which couple to the electronic transition [27 28]. Indeed, absorption bands of naphtalene C=C and C=O groups are found in the range 1400-1700 $cm^{-1}$ in PEN, i.e. 0.17-0.21 eV [29].

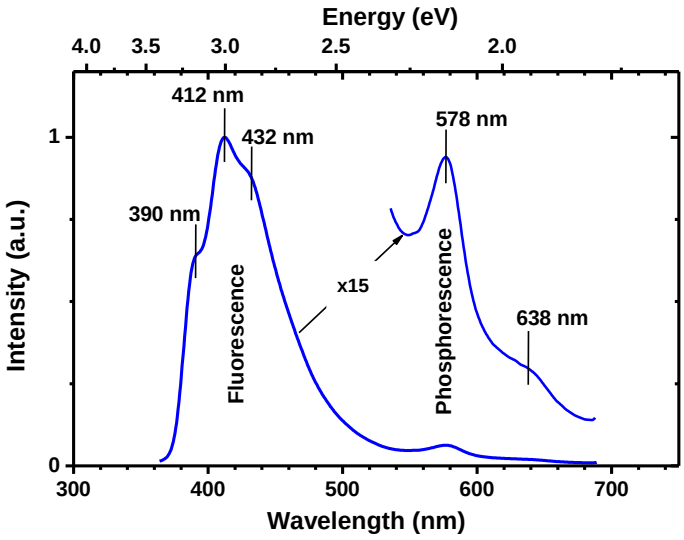


**Fig. 6.** PL emission spectrum of 25 µm-thick PEN at low temperature. Excitation is at 350 nm

The fact that emission involves excimeric emission, i.e. interaction between adjacent naphthalene rings pushes to the importance of simulating interchain interactions. In fluorescence lifetime measurements, it was reported that in the solid state of amorphous PEN, one don't know where the excimer starts to emit; however, at 390 nm the fluorescence decay curve is dominated by monomer emission [30]. Hence, the band at 390 nm is possibly related to monomeric emission and the longer wavelength ones to excimeric emission.

The weak emission peaking at 578 nm (2.15 eV) with shoulder at 638 nm (1.95 eV) is the $^{3}(\pi, \pi^*)$ phosphorescence transition originating from the monomeric units [31]. The probability of phosphorescence transition is low because there is a weak coupling between the states $^{1}(\pi, \pi^*)$ and $^{3}(\pi, \pi^*)$. The energetic levels computed for a group of three adjacent molecules, give a value of fluorescence emission at 3.03 nm (409 nm) which is near the experimental value. Optical absorption edges ($\pi > \pi^*$ transitions) are located at 3.0 eV (S1), 4.4 eV (S2) and 6.0 eV (S3), i.e. very near the experimental values see Table I. Adding the levels due to ($n > \pi^*$) transition, singlet and triplet, related to the non-bonding electron on the oxygen atoms leads to the scheme proposed in Fig. 7.a. One of the striking conclusions is that exciton S3 is dissociative because the excited level is above the vacuum level. The orbital is not along the macromolecule but lies outside. It is easily dissociated by the electric field for example.

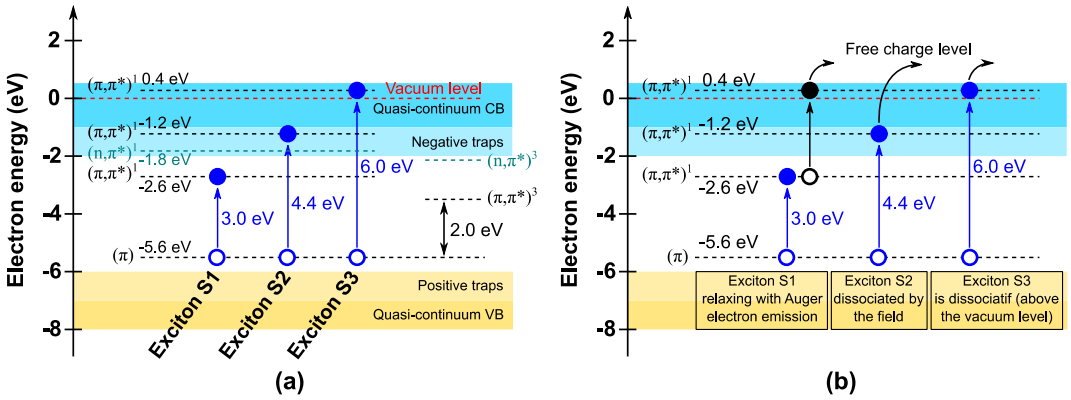


**Fig. 7.** Schematic representation of the energetic levels due to π and n levels of the PEN molecule. (a) electronic transitions responsible for optical absorption; (b) Electronic transitions explaining charge detrapping and PSD upon irradiation.

### Mechanisms involved in PSD

From this scheme, one can postulate several mechanisms explaining the PSD phenomenon –see Fig. 7b. Exciton S1 can relax through the emission of an Auger electron [32]. Exciton S2 can be dissociated by the electric field, the pair of charges being weakly bound and all the more for exciton S3. This mechanism is well documented for organic semi-conductors for example [33]. All these processes lead to a net balance of one electronic charge that contributes to the external current. PSD spectra shown in Fig. 3 under positive poling condition demonstrate that irradiation at 210 nm gives rise to a negative current. This is expected as described in the section below.

### PSD current and poling polarity

The cartography of Fig. 2 shows that a high density of positive charges accumulated near the anode during positive poling (see for example 200 kV/mm applied field) as well as negative charges near the cathode. The electric field is therefore lowered near the electrodes and enhanced in the volume during poling, a typical situation when bi-polar injection occurs as schematically represented in Fig. 8-a. In depolarization, the space charge field induces a negative field at the electrodes (Fig. 8-b). Under irradiation, and due to the small penetration depth of the light, free electrons are generated in the immediate vicinity of the electrode where the field is negative (Fig. 8-b). They are pushed away from the electrode inducing a negative current in the external circuit.

According to this scheme, changing the polarity of the applied voltage should give a positive current in the external circuit because the space charge induces a positive field at the electrodes under depolarization (Fig. 8-d). This is experimentally observed as shown in Fig. 3 except for the 207 nm PSD peak. Moreover, up to about 100 kV/mm, the 207 nm PSD peak is still negative when changing continuously from a positive poling to a negative one. This is due to the remnant space charge that is still positive even under negative poling maintaining a negative field at the electrodes as schematically represented in Fig. 8-c. This is also clearly shown in Fig. 2 where positive charges are detected near the negatively biased electrode up to a field of about 100 kV/mm.

These schemes are confirmed by the computation of the electric field derived from our space charge measurements. Residual electric fields one hour after depolarization at 200 kV/mm and -200 kV/mm are plotted in Fig. 9. The field tends to be negative in the immediate vicinity of the electrode, and positive elsewhere at +200 kV/mm, as opposed to the case at -200 kV/mm.

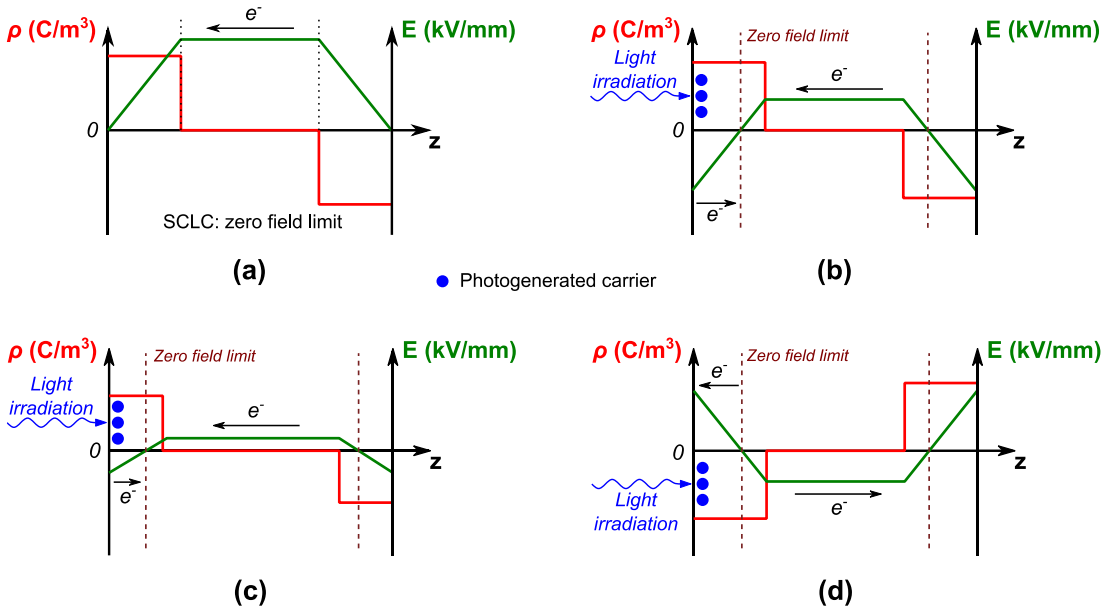


**Fig. 8.** Schematic representation of the electric field and charge state in different situations with (a, b) positive and (c, d) negative voltage (pre-)applied to the irradiated electrode. The arrows indicate the movement of the electrons. (a)-Field under condition of bipolar injection; (b)-Space charge field in depolarization after application of high field; (c)-Net remnant space charge after polarity inversion of the applied voltage when the previously injected charges under positive polarity have not been compensated/recombined by the injection of negative charges under negative polarity; (d)-Space charge field once a strong negative poling is applied to the irradiated electrode.

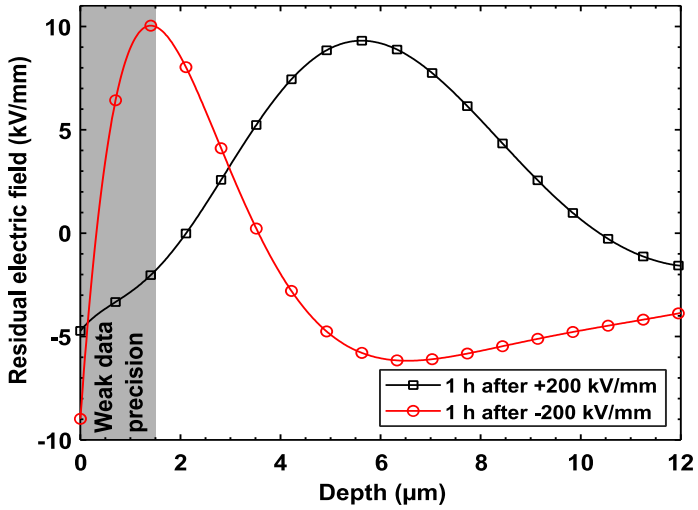


**Fig. 9.** Residual electric field after one hour in depolarization at +/-200 kV/mm

There is still to explain the absence of the 207 nm PSD peak when the irradiated electrode is negatively biased. Also, the other PSD peaks are of much lower magnitude under negative voltage when compared to positive voltage. Consider the situation under positive bias voltage (with reference to the irradiated electrode) schematically represented in Fig. 10-a. According to the scheme presented in Fig. 6, one notes that levels S0 and S1 do not provide efficient hole and electron traps respectively contrary to levels S2 and S3 which are efficient electron traps. In the condition of bipolar injection, the majority carriers in the vicinity of the positively biased electrode are holes with high degree of occupation of the shallow and deep hole traps (yellow areas). Levels S1, S2 and S3 associated with PSD peaks as shown in Fig. 10-a are occupied by minority carriers (electrons injected at the cathode that transit through the thickness of the PEN film). The probability of excitons creation is proportional to the number of electrons available on level S0 times the number of available sites on levels S1, S2 and S3 times the photons flux in the irradiation light. As a result, excitons S1 have a higher probability to be created than excitons S2 which is consistent with the relative magnitude of the associated PSD peaks. Excitons

S3 also have a high probability and contribute strongly to the PSD current because level S3 is dissociative and excited in the immediate vicinity of the irradiated electrode. The contribution of S3 to the current is much higher than that of excitons S1 and S2 because there is no Auger effect involved in the generation of a free charges from exciton S3.

Now consider the case of a negative applied voltage as depicted in Fig. 10-b. The majority carriers in the vicinity of the cathode are now electrons and they populate levels S3, S2 and S1, the latter to a lower degree due to its position in the band gap. Level S3 is the more densely populated, followed by level S2. Minority carriers are holes being injected at the anode and drift towards the cathode. They occupy mainly the hole traps located between -6 eV and -8 eV, and also level S0 to a lower extent. Excitons S1 and S2 can be excited because level S0 is almost filled by electronic charges and there are some available sites at level S1, and to a less extent at level S2. However, level S3 is occupied by a large number of electrons which opposes the electronic transition from S0 to S3 associated with exciton S3. This provides an explanation of the relative magnitude of PSD peaks S1 and S2, and the absence of peak S3 in the spectrum. The explanation is certainly not definitive as the density of trapped electrons must be high to impact exciton formation. In the field of organic electronics, hole traps are often considered as detrimental to the yield of devices [34]. Hole traps are known to interact with excitons, involving their quenching, as a competitive mechanism to field-induced exciton dissociation. One possible exciton quenching path leads to the formation of a free hole [35]. This could constitute an alternative reason for the difference in behavior for positive and negative polarity.

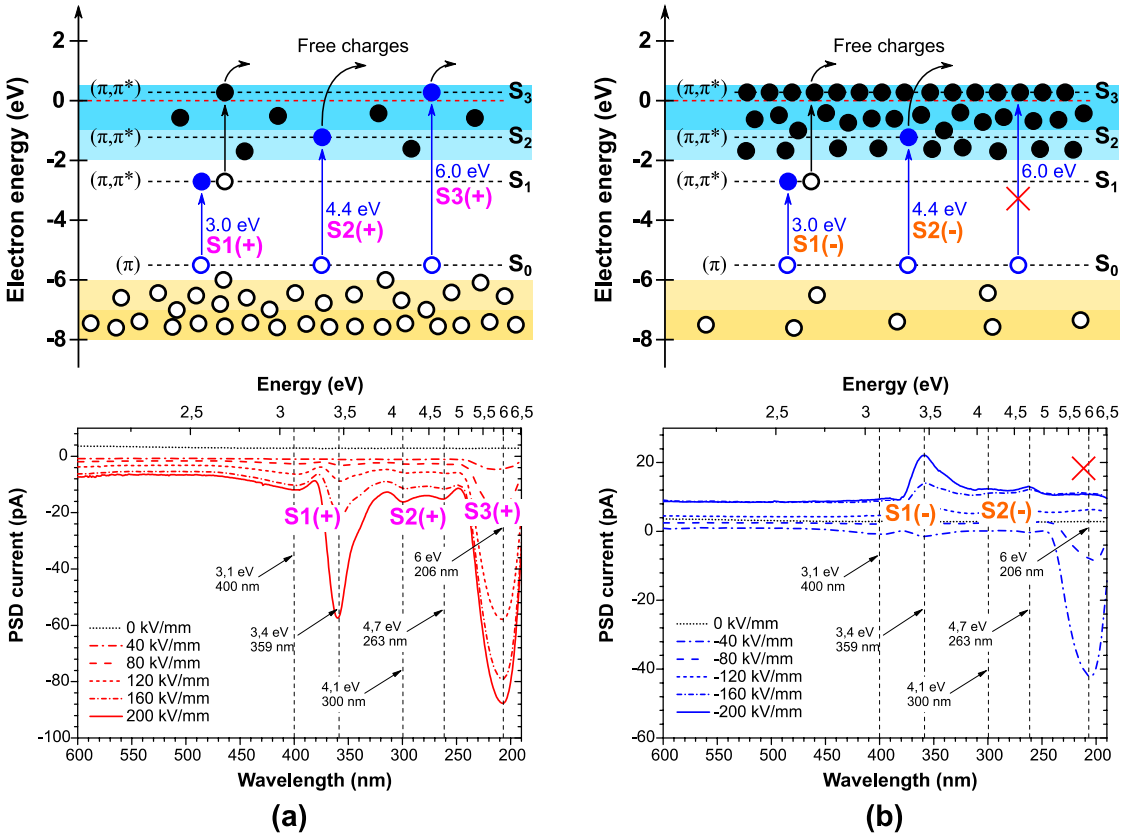


**Fig. 10.** Schematic representation of the electronic levels occupation when the irradiated electrode is positively (a) and negatively (b) biased and associated PSD spectrum. Transitions associated with excitons S1, S2 and S3 are indicated with their PSD peaks counterpart. Electrons are plotted in blue and black. Holes in white.

### Electronic levels and PEN optical emission under various stresses

Optical emission spectra of PEN were recorded when submitted to stresses of different nature: under photon irradiation –photoluminescence PL; under electric field –electroluminescence EL; after charging by application of an electric field –charge recombination induced luminescence RIL; after charging by contact with a cold plasma –plasma induced luminescence PIL; upon heating after charging –thermoluminescence TL; under electron

irradiation –cathodoluminescence CL. All these spectra present specific characteristics which provide the opportunity to evaluate the model of electronic levels of PEN as presented in Fig. 7.

*Photoluminescence*: the PL emission spectrum obtained at low temperature has already been presented in Fig. 6. It is reproduced in Fig 11-a for the sake of clarity with adding the response at room temperature. It is characterized by a strong fluorescence and a weak phosphorescence detected only at low temperature. The emission spectrum is unchanged for light excitation in the range 200 nm to 380 nm. As previously discussed the spectrum was assigned to the fluorescence transition of an excimer state formed between two adjacent naphthalene-dicarboxylate units, the phosphorescence transition originating from the monomeric units. We used the PL spectrum to complete the scheme derived from ab-initio calculations. Under light irradiation, levels S1 to S3 can be populated depending on the wavelength of the light. Internal conversion releases the energy down to level S1, then to the ground state with emission of fluorescence (singlet to singlet transition). However, the level $^1$(n, π*) can also be populated upon light irradiation which provides the possibility of inter-system crossing between this level and the $^3$(n, π*) due to their energy matching, contrary to the energy mismatch between $^1$(π, π*) and $^3$(π, π*). This explains the presence of a strong fluorescence and a weak phosphorescence in the PL spectrum.

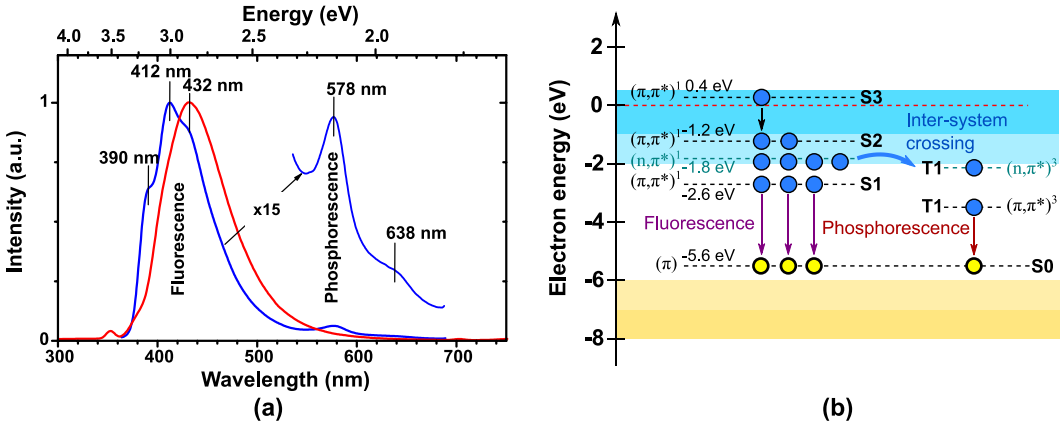


**Fig. 11.** Energetic processes associated with photoluminescence in PEN. (a) Photoluminescence spectra of 25 µm-thick PEN at room temperature (red) and at liquid nitrogen temperature (blue) upon excitation at 350 nm; (b) associated electronic transitions.

*Electroluminescence and delayed luminescence (or RIL)*: typical electroluminescence spectra are shown in Fig. 12-a at different DC fields [8]. Under moderate field of 250 kV/mm the spectrum is organized around two components at 450 nm and 578 nm, with a shoulder at 675 nm. Increasing the field up to 400 kV/mm leads to the predominance of the component at 618 nm with a vanishing of the 450 nm component. The 578 nm component is the phosphorescence of the PEN which has therefore a major contribution to the EL spectrum. Since EL is associated with a degradation of the molecules with signature at 618 nm and 675 nm [8], the scheme of the electronic levels introduced in Fig. 7 cannot be used to interpret these transitions. However, the scheme can be useful to explain the predominance of PEN phosphorescence in the EL spectrum. A tentative explanation is proposed in Fig. 12-b remembering that EL is excited upon charge recombination and/or impact excitation in a regime where bipolar charging is achieved. Electrons and holes are trapped on levels with negative and positive affinity respectively. Level S1 is not an efficient trap for electrons and is therefore not populated to a large extent. It follows that electron/hole recombination will preferentially occur via inter-system crossing between $^1$(n, π*) and $^3$(n, π*) which leads to phosphorescence emission.

The component at 450 nm visible in the spectrum at moderate field could be a fluorescence shifted to the red due to specific configurations of the PEN molecules mediated by the electric field, or even new chemical entities created by bond breaking reactions. Under very high field (400 kV/mm), levels S1, S2 and S3 could be depopulated upon impact of hot electrons or field dissociation. Impact will raise secondary electrons to higher energetic levels, field dissociation will generate pair of charges. Because triplet excitons have stronger binding energy they will be less sensitive to electron impact or field dissociation. This would lead to a drastic decrease of the fluorescence component vs. the phosphorescence component as observed experimentally–see Fig. 12-c.

It was also reported that optical emission is recorded after voltage application for quite a long time (several tens of seconds), called “delayed luminescence” [23], and checked that the emission was not due to long lived excited states involved in phosphorescence emission. The emission spectrum of this “delayed luminescence” is similar to the one obtained in EL at 300 kV/mm –see Fig. 12-d. The only mechanism at play in such situation is radiative charge recombination (from which comes the term Recombination-Induced Luminescence) between trapped carriers because high field effects such as those evoked at 400 kV/mm cannot occur in volt off. It is worth pointing out that the component in the fluorescence region is detected in the delayed luminescence spectrum. The scheme will therefore be the one presented in Fig. 12-b operating at moderate field.

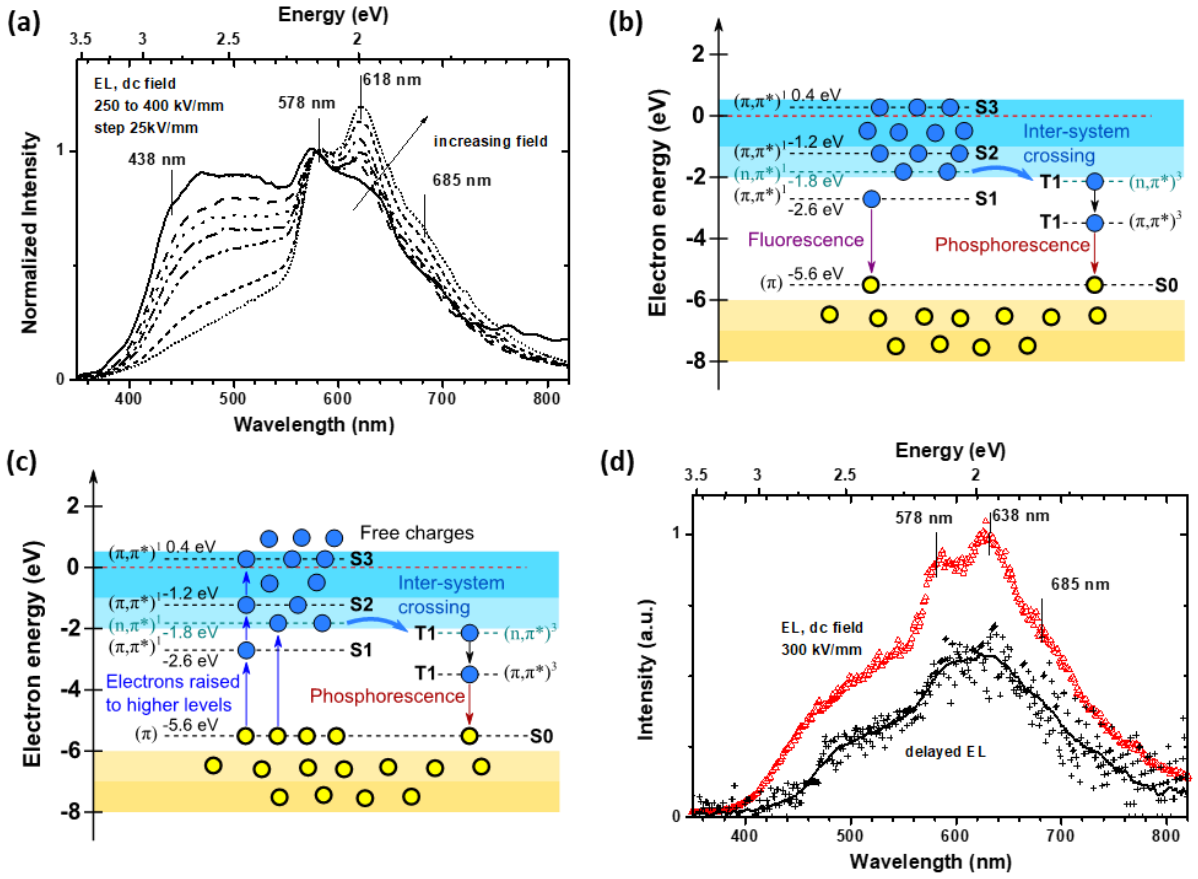


**Fig. 12.** Electroluminescence spectra under DC field and schematic representation of the electronic transitions involved. (a)-Emission spectra vs. electric field under DC stress [8]; (b)-Electronic transitions involved at moderate field (250 kV/mm) explaining the predominance of phosphorescence vs. fluorescence; (c)-Electronic transitions involved at very high field (400 kV/mm) explaining the absence of emission in the fluorescence domain. Electrons and holes are represented in blue and yellow respectively; (d)-Emission spectra of delayed luminescence and electroluminescence at 300 kV/mm [23].

*Charge recombination-induced luminescence and thermoluminescence:* Bipolar charging can also be achieved contacting the PEN film by a cold plasma powered under AC voltage under inert atmosphere and carefully controlled conditions [36]. The plasma deposits positive and negative charges at the surface and in the first layers a few microns in depth. Luminescence is emitted after discharge switch-off for time up to several tens of minutes. Different contributions have been identified in the luminescence but the long lasting component is due to charges that recombine [11]. The spectra shown in Fig. 13-a are characteristic of charge recombination: they have been acquired either isothermally at ≈-120 °C or during heating, corresponding to thermoluminescence. The spectra obtained at different times along the luminescence decay stay perfectly the same from 5 s to several minutes after the discharge and match the photoluminescence emission with however an enhanced phosphorescence vs. fluorescence.

When increasing the temperature from ≈-120 °C to ≈-50 °C (the temperature was only approximately controlled) the spectra are still organized along the fluorescence/phosphorescence of the PEN molecules with enhancement of the phosphorescence vs. fluorescence when increasing the temperature. The spectra can be interpreted on the basis of the scheme of Fig. 12-b that explains the phosphorescence enhancement in charge recombination phenomena. At a given temperature, spectra taken at different times along the luminescence decay do not change giving the evidence that the process of recombination stays the same. Upon temperature increase, phosphorescence is enhanced but the reasons are not clear: charge trapping imparts change in the probability of inter-system crossing, or triplet-triplet annihilation is at play for producing fluorescence.

One important conclusion is that charge recombination following bipolar PEN charging under mild conditions, i.e. without the mediation of high field, can be explained on the ground of electronic levels of the very molecule. There is no sign of material degradation leading to the formation of by-products and therefore the mediation of new energy levels in the process. This is obviously contrary to the case of electroluminescence where new optical signatures evidenced the creation of new electronic levels.

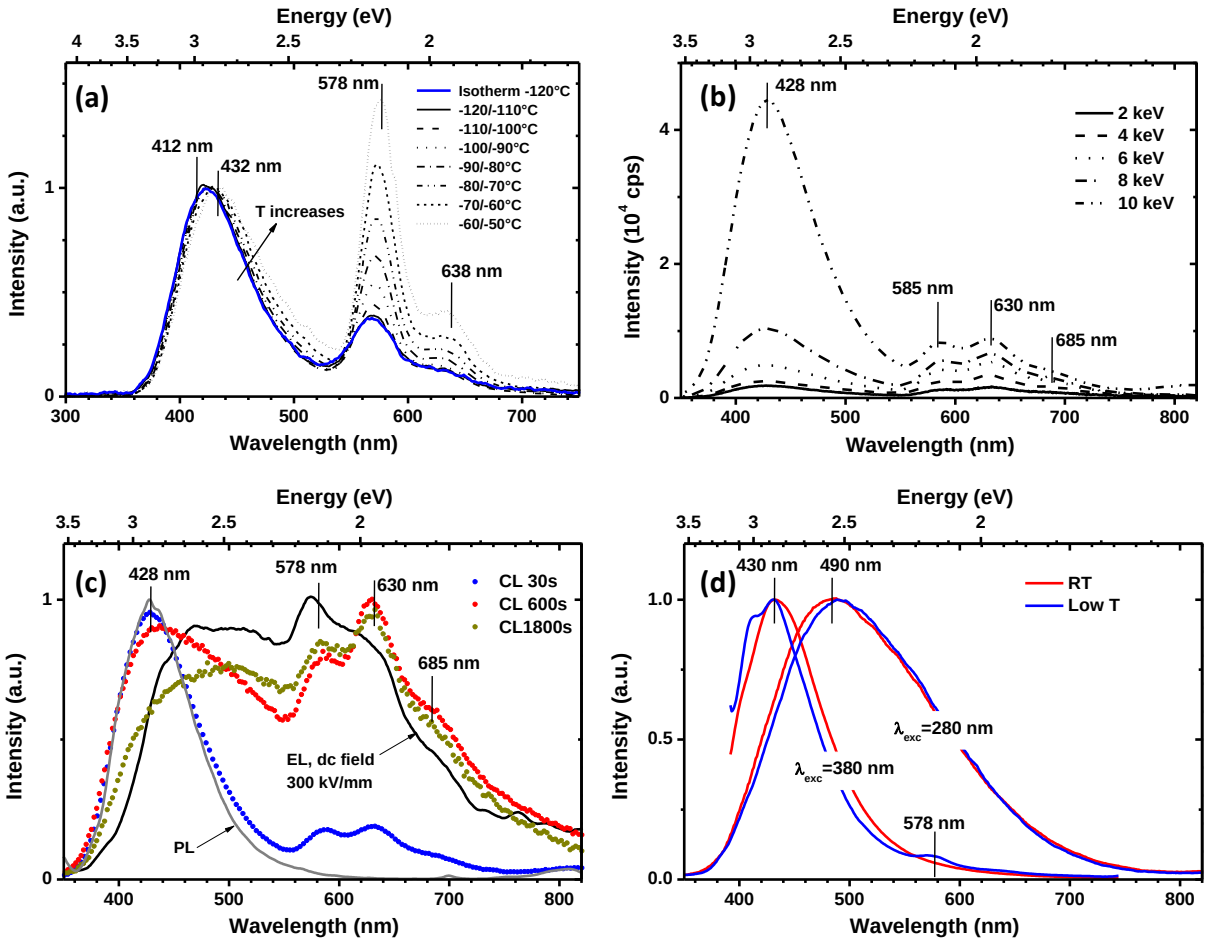


**Fig. 13.** (a) Luminescence spectra following charge recombination after contact of the film with a cold plasma, measured isothermally at ≈-120 °C and in thermoluminescence during heating from ≈-120 °C to ≈-50 °C (Not previously published); (b): Cathodoluminescence spectra for different energy of the electron beam at short time [37]; Comparison of CL spectra after different irradiation times under 10 keV electrons compared to EL and PL spectra; (d) Photoluminescence spectra at 25°C and -130 °C of PEN aged under UV light for 50 h using different excitation wavelengths. At an excitation wavelength of 280 nm only the film surface is probed [38].

*Cathodoluminescence:* Films of PEN have been subjected to electronic irradiation in vacuum with energy up to 10 keV (electron current of the order of 0.5 μA/mm²) -so called cathodoluminescence CL [37]. It follows a set of possible excitation mechanisms among which impact ionization at moderate kinetic energy (order of 15 eV) with secondary electrons emission, impact excitation (10 eV) with generation of excitons, quasi-elastic scattering with phonons (energy < 10 eV), and finally electron trapping at thermal energy. Because the electron beam is able to

ionize PEN molecules, bipolar charging is also achieved in these conditions. The CL spectra are shown in Fig. 13-b as a function of the energy of the beam and in Fig. 13-c as a function of the time of irradiation at a constant energy of 10 keV. The spectra are organized around 4 components: a first one laying in the domain of the fluorescence emission and the three others in the phosphorescence domain. The 430 nm fluorescence component of PEN is visible in the CL spectra for any energy of the beam at short time (Fig. 13-b), but evolves quickly as a function of the irradiation duration –see Fig. 13-c. It shifts to the red, broadening and peaking at 500 nm for 1800 s irradiation. It seems therefore that the initial structure responsible for PEN fluorescence is affected by the energy of the beam and evolves towards a new structure emitting at 500 nm. The component of the cathodoluminescence in the domain of PEN phosphorescence appears as a structure with three maxima at about 585 nm, 630 nm and 675 nm. Note that the phosphorescence of the PEN as shown in Fig. 6-a exhibits a doublet at 578 nm and 638 nm that is also visible in recombination induced luminescence spectra in Fig. 13-a.

It is clear that a scheme as shown in Fig. 6 cannot explain the time evolution of the cathodoluminescence spectrum that provides the evidence of chemical changes and therefore a modification of the electronic levels involved in light emission. Interestingly, the electroluminescence spectrum under DC stress has been plotted in the same Fig. 13-c. It is striking that the components of the EL emission are the same as those of the CL obtained for long irradiation time. This demonstrates that EL signs molecular degradation reactions.

An insight on the nature of the “new” component in EL or CL spectra at 500 nm can be attempted by investigating photoluminescence of UV-“aged” PEN. By investigating the photoluminescence at different times under UV irradiation, it could be possible to unravel this “new” component. This has been done in [38] and the evolution of photoluminescence has been plotted in Fig. 13-d. It can be seen that the fluorescence of PEN is shifted to the red with an emission maximum at 500 nm upon aging. This component is also present in EL and CL. Several works have focused on surface modification of PEN with either plasma attack in air, oxygen, or nitrogen atmosphere or UV-oxidation [39 40 41]. Elemental surface analysis by XPS and other techniques revealed the incorporation of new chemical groups at the surface, as C=O, O–C–O, O=C–O and –C(O)–O–C(O)– bonds and partial destruction of the aromatic rings. Table II sums-up our interpretation of the luminescence spectrum of PEN using different sources. The fact that the bands that we have associated to material degradation are revealed by PL in UV-aged materials and in EL but not in CL in the first instant of irradiation points to mostly surface degradation of the PEN films. The electron beam produces relatively in-depth modification while EL would be mostly a surface effect. The new molecular groups are to be researched among aromatic rings combined to candidate oxidized groups identified by surface analysis techniques. Admittedly so far, we have not a definitive assignment of the exact nature of these groups.

**Table II.** Emission bands detected in PEN using different techniques and their assignment.

| Emission (nm) | PL | PIL-TL | EL | CL | Assignment |
|---|---|---|---|---|---|
| 430 (RT); 390(s)-412-432(s) (LT) | X | X | -- | X | Fluorescence involving $^1(\pi\text{-}\pi^*)$ |
| 490 (broad) | X[i)] | | X | X[ii)] | Fluorescence due to forming or existing degradation products |
| 578 (RT); 578, 638 (LT) | X | X | | | Phosphorescence involving $^3(n\text{-}\pi^*)$ |
| 630, 685 (RT) | | | X | X | Phosphorescence due to forming degradation products |

RT: room temperature; LT: low temperature; (s): shoulder; (i) Only after UV-ageing of the film; (ii) Upon long exposure to e-beam

## IV CONCLUSION

PSD peaks are very often associated with trap depths giving values, of the order of several eV, that are much higher than trap depths derived from competitive techniques that are of the order of 1 eV or less. We have shown that the PSD peaks of PEN are associated with the optical absorptions of the material. There is no reason why this energy will give an idea of trap depths. Relying on photoluminescence and recent calculations of molecular dynamics on PEN, we proposed a new scheme of the electronic levels associated with the orbitals π and n of the

molecule. It gives a basis to interpret PSD peaks and to propose mechanisms by which light irradiation leads to material discharging. Irradiation with energetic light (about 200 nm) leads to a peculiar behavior which is explained by the fact that such energy generates weakly bounded excitons that are prompt to dissociation in the absorbing region, i.e. the immediate vicinity of the irradiated electrode. Other electrode effects could also be influential but this would need playing with electrode parameters, not achieved in our study.

On the basis of the new scheme, we were able to discuss the emission spectra of luminescence excited by different stresses. It is clear that some of the stresses investigated in this study promote bond scission reactions and formation of new chemical species (high field application, electronic irradiation and UV irradiation). The scheme is obviously not able to fully explain the emission spectra in these cases. However, when mild stresses unable to generate bond breaking reactions are at play (charge recombination, mild UV irradiation, thermal activation), the scheme gives a basis of interpretation. To go further, molecular dynamics calculation on these new entities would be of great help together with computation of excited states.

**REFERENCES**


1 M. Campajola, F. Di Capua, P. Casolaro, E. Sarnelli, and A. Aloisio, "Radiation damage in polyethylene naphthalate thin-film scintillators", *Materials*, vol. 15, p. 6530, 2022. https://doi.org/10.3390/ma15196530

2 L. Caliari, P. Bettacchi, E. Boni, D. Montanari, A. Gamberini, L. Barbieri, and F. Bergamaschi, "KEMET SMD film capacitors for high temperature applications." *IMAPSource Proceedings*, vol. HITEN, pp. 13–24, 2013: https://doi.org/10.4071/HITEN-MA13.

3 D. Mary, M. Albertini, and C. Laurent, "Understanding optical emissions from electrically stressed insulating polymers: electroluminescence in poly (ethylene terephthalate) and poly (ethylene 2, 6-naphthalate) films", *J. Phys. D: Appl. Phys*, vol. 30, pp. 171-184, 1997. https://doi.org/10.1088/0022-3727/30/2/004

4 J. L. Augé, G. Teyssedre, C. Laurent, T. Ditchi, and S. Holé, "Combined electroluminescence and charge profile measurements in poly (ethylene-2, 6-naphthalate) under a dc field", *J. Phys. D: Appl. Phys*, vol. 33, pp. 3129-3138, 2000. http://doi.org/10.1088/0022-3727/33/24/301

5 M. Ieda, Y. Takai, and T. Mizutani, "Photoconduction processes in polymers", in *Developments in Photochemistry*, Part III, Applied Science Publishers, New Jersey, p. 93, 1982.

6 A. Laskarakis and S. Logothetidis, "Study of the electronic and vibrational properties of poly (ethylene terephthalate) and poly (ethylene naphthalate) films", *J. Appl. Phys.*, vol. 101, p. 053503, 2007. https://doi.org/10.1063/1.2709572

7 J. Davenas, G. Boiteux, G. Seytre, and C. Jardin, "Role of the structure on the photo and cathodo-luminescence of poly (ethylene naphthalate): PEN", *Synthetic metals*, vol. 115, pp. 83-87, 2000. https://doi.org/10.1016/S0379-6779(00)00352-0

8 G. Teyssedre, D. Mary, C. Laurent, and C. Mayoux, "Optical emission due to space charge recombination in insulating polymers: An insight into electrical ageing", in *Space charge in solid dielectrics*, Ed. J.C. Fothergill and L.A. Dissado, Dielectrics Society, Leicester, Chap.26, pp. 285-302, 1998.

9 P. Ma, Y. Zhang, S. Holé, F. Zheng, M. Gu, and Z. An, "Analysis and interpretation of photo-stimulated discharge spectrum for polypropylene films under different electric and geometrical conditions", *J. Electrostatics,* vol. 84, pp. 128-134, 2016. https://doi.org/10.1016/j.elstat.2016.10.004

10 D. Mendoza-Lopez, G. Teyssedre, L. Berquez, and L. Boudou, "Study of trapping process in BOPP by coupled space charge and photo-stimulated discharge techniques", *Proc. IEEE 4th International Conference on Dielectrics,* Palermo, Italy, pp.376-379, 2022. https://doi.org/10.1109/ICD53806.2022.9863568

11 G. Teyssedre, F. Zheng, L. Boudou, and C. Laurent, "Charge trap spectroscopy in polymer dielectrics: a critical review", *J. Phys. D: Appl. Phys.*, vol. 54, p. 263001, 2021. https://doi.org/10.1088/1361-6463/abf44a

12 I. G. Scheblykin, A. Yartsev,T. Pullerits, V. Gulbinas, and V. Sundstrom, "Excited state and charge photogeneration dynamics in conjugated polymers", *J. Phys. Chem. B*, vol. 111, pp. 6303-6321, 2007. https://doi.org/10.1021/jp068864f

13 D. Liraz and N. Tessler, "Charge dissociation in organic solar cells—from Onsager and Frenkel to modern models", *Chem. Phys. Rev.*, vol. 3, p. 031305, 2022. https://doi.org/10.1063/5.0099986

14 T. Takada, "Studies on space charge accumulation properties in dielectric materials," *Proc. 2019 2nd International Conference on Electrical Materials and Power Equipment (ICEMPE)*, Guangzhou, China, pp. 1-8, 2019. https://doi.org/10.1109/ICEMPE.2019.8727258

15 T. Takada, "Application examples of quantum chemical calculation", in *Electric Charge Accumulation in Dielectrics: Measurement and Analysis*, Singapore: Springer Nature Singapore, pp. 243-294, 2022.

16 J. Hornak, P. Kadlec, J. Kopřiva, and R. Polanský, "Dielectric, structural and mechanical properties of thermally aged biaxially oriented polymeric substrates for flexible electronics", Polymer Degrad. Stab., vol. 199, n° 109906, 2022. https://doi.org/10.1016/j.polymdegradstab.2022.109906

17 D. Mendoza-Lopez, L. Berquez, L. Boudou, and G. Teyssedre, "Measurement setup to simultaneously explore the location and energy of trapped charges in thin polymer films", *Rev. Sci. Instrum.*, vol. 94, p. 084705, 2023 https://doi.org/10.1063/5.0159025

18 A. Velazquez-Salazar, L. Berquez, and D. Marty-Dessus, “Thermal modeling and calibration in (F)LIMM using an external bias field: Theory and experiment,” *IEEE Trans. Dielectr. Electr. Insul.*, vol. 25, pp. 783–790, 2018. https://doi.org/10.1109/TDEI.2017.007029

19 G. Teyssèdre, C. Laurent, and B. Qiao, "Advanced characterization techniques based on luminescence in XLPE and modified XLPE", in "Crosslinkable polyethylene based blends and nanocomposites", Materials Horizons: From Nature to Nanomaterials, J. Thomas, S. Thomas, Z. Ahmad (Eds), Springer Singapore, ISBN: 978-981-16-0486-7, Chap. 6, pp. 99-157, 2021

20 H.J.C. Berendsen, D. van der Spoel, and R. van Drunen, "GROMACS: A message-passing parallel molecular dynamics implementation", *Computer Phys. Comm.*, vol. 91, pp. 43-56, 1995. https://doi.org/10.1016/0010-4655(95)00042-E

21 M. J. Abraham, T. Murtola, R. Schulz, S. Páll, J. C. Smith, B. Hess, and E. Lindahl, "GROMACS: High performance molecular simulations through multi-level parallelism from laptops to supercomputers", *SoftwareX*, vol. 1–2, pp. 19-25, 2015. https://doi.org/10.1016/j.softx.2015.06.001

22 H. Nakamura et al, "Optimized mounting of a polyethylene naphthalate scintillation material in a radiation detector", Appl. Rad. Isotopes, vol. 80, pp. 84-87, 2013. https://doi.org/10.1016/j.apradiso.2013.06.011

23 G. Teyssedre, D. Mary, and C. Laurent, “Analysis of the luminescence decay following excitation of polyethylene naphthalate films by an electric field”, *J. Phys. D: Appl. Phys.*, vol. 31, pp. 267-275, 1998. http://dx.doi.org/10.1088/0022-3727/31/3/003

24 . J. L. Street and G. B. Brédas, "Electronic structure of polystyrene: A valence effective Hamiltonian theoretical study," *J. Chem. Phys.*, vol. 82, p. 3284, 1985. https://doi.org/10.1063/1.448226

25 M. Fukuma, G. Teyssedre, C. Laurent, and K. Fukunaga. "Millisecond time range analysis of space charge distribution and electroluminescence in insulating polymers under transient electric stress". J. Appl. Phys., vol. 98, p. 093528, 2005. http://dx.doi.org/10.1063/1.2128050

26 H. Hashimoto, M. Hasegawa, K. Horie, T. Yamashita, H. Ushiki, and I. Mita, "Fluorescence study of thermotropic liquid-crystalline polyesters", *J. Polym. Sci.: Phys.*, vol. 31, pp. 1187-1196, 1993. https://doi.org/10.1002/polb.1993.090310913

27 H. J. Pownall and J. R. Huber, "Absorption and emission spectra of aromatic ketones and their medium dependence. Excited states of xanthone", *J. Am. Chem. Soc.*, vol. 93, pp. 6429–6436, 1971. https://doi.org/10.1021/ja00753a016

28 M.J. van der Burgt, A.H. Huizer, C.A.G.O. Varma, B.D. Wagner, and J. Lusztyk, "Evidence for molecular distortion involving the carbonyl group in triplet states of carbonyl derivatives of naphthalene obtained from time resolved vibrational spectroscopic studies", *Chem. Phys.*, vol. 196, pp. 193-210, 1995. https://doi.org/10.1016/0301-0104(95)00117-7

29 D.D.B. Jung, D. Bhattacharyya, and A.J. Easteal, "Spectroscopic analysis of poly(ethylene naphthalate)–poly(butylene terephthalate) blends", *J. Appl. Polym. Sci.*, vol. 106, pp. 1860-1868, 2007. https://doi.org/10.1002/app.26736

30 C. Spies and R. Gehrke, "Time-resolved fluorescence measurements on poly(ethylene naphthalene-2,6-dicarboxylate)", *Macromolecules*, vol. 30, pp. 1701-1710, 1997. https://doi.org/10.1021/ma960795n

31 P.S.R., Cheug, C.W. Roberts, and K.B. Wagener, "Synthesis, photodegradation, and energy transfer in a series of poly(ethylene terephthalate-co-2, 6-naphthalenedicarboxylate) copolymers," *J. Appl. Polym. Sci.*, vol. 24, pp. 1809-1830, 1979. https://doi.org/10.1002/app.1979.070240804

32 J. P. Jones, J. P. Llewellyn, and T. J. Lewis, "The contribution of field-induced morphological change to the electrical aging and breakdown of polyethylene", *IEEE Trans. Dielectr. Electr. Insul.,* vol. 12, pp. 951-966, 2005. https://doi.org/10.1109/TDEI.2005.1522189

33 M. Deussen, M. Scheidler, and H. Bässler. "Electric field-induced photoluminescence quenching in thin-film light-emitting diodes based on poly (phenyl-p-phenylene vinylene)", *Synthetic Metals*, vol. 73, pp. 123-129, 1995. https://doi.org/10.1016/0379-6779(95)03307-6

34 I. Rörich, Q. Niu, B. van derZee, E. del Pino, N.I. Crăciun, C. Ramanan, and P.W.M. Blom, "Exciton quenching due to hole trap formation in aged polymer light-emitting diodes", *Adv. Electron. Mater.*, vol. 6, p. 1700643, 2020. https://doi.org/10.1002/aelm.201700643

35 N. H. Hansen, C. Wunderlich, A. K. Topczak, E. Rohwer, H. Schwoerer, and J. Pflaum, "Exciton interaction with a spatially defined charge accumulation layer in the organic semiconductor diindenoperylene", *Phys. Rev. B*, vol. 87, p. 241202(R), 2013. https://doi.org/10.1103/PhysRevB.87.241202

36 G. Teyssedre, L. Cisse, C. Laurent, F. Massines, and P. Tiemblo, "Spectral analysis of optical emission due to isothermal charge recombination in polyolefins", *IEEE Trans. Dielectr. Electr. Insul.*, vol. 5, pp. 527-535, 1998. https://doi.org/10.1109/94.708268

37 G. Teyssedre, J.L. Franceschi, and C. Laurent, "Cathodo- and electro-luminescence spectra in insulating polymers: a parallel approach for inferring electrical ageing mechanisms", *Proc. IEEE Int. Conf. on Electrical Insulation and Dielectric Phenomena (CEIDP)*, Vancouver, Canada, pp. 824-827, 2007. https://doi.org/10.1109/CEIDP.2007.4451566

38 G. Teyssedre, D. Mary, and C. Laurent, "Electroluminescence and photoluminescence of UV-aged Poly(ethylene naphthalate) films", *IEE. Proc.-Sci. Meas. Technol.*, vol. 150, pp. 83-88, 2003. https://doi.org/10.1049/ip-smt:20030020

39 A. Vesel, K. Eleršič, I. Junkar, and B. Malič, "Modification of a polyethylene naphthalate polymer using an oxygen plasma treatment", Materials and Technology, vol. 43, pp. 323-326, 2009

40 M. Kormunda, T. Homola, J. Matousek, D. Kovacik, M. Cernak, and J. Pavlik, "Surface analysis of poly(ethylene naphthalate) (PEN) films treated at atmospheric pressure using diffuse coplanar surface barrier discharge in air and in nitrogen", Polymer Degradation and Stability, vo. 97, pp. 547-553, 2012. https://doi.org/10.1016/j.polymdegradstab.2012.01.014

41 E. Al AbdulalE, A. Bailey, M. Mehan, S.K. Gupta, X. Li, M. Toro, and G.A. Takacs, "Surface modification of PEN treated with ozone and UV photooxidation", Surface Innovations, vol. 4, pp. 39–47, 2016. http://dx.doi.org/10.1680/jsuin.15.00018